

Density functional theory investigations into the magnetic ordering of U_3O_8 Sara B. Isbill , Ashley E. Shields, J. L. Niedziela, and Andrew J. Miskowiec 

Nuclear Nonproliferation Division, Oak Ridge National Laboratory, Oak Ridge, Tennessee 37831, USA

 (Received 16 March 2022; revised 8 August 2022; accepted 8 September 2022; published 19 October 2022)

Density functional theory (DFT) has been highly successful in supporting experimental materials science; however, a correct electronic ground state is required to realize the full theoretical capacity of DFT. The uranium oxides, $\alpha-U_3O_8$ in particular, are simultaneously technologically important materials and theoretically challenging for DFT because the uranium magnetic ground state is not obvious. This is true for both experiment and theory—magnetic susceptibility measurements indicate an antiferromagnetic (AFM) ground state with transitions near 4.2 and 8.0 K, but the ordering itself is not known. Theoretical literature reports are in contradiction, with independent studies finding paramagnetic, ferromagnetic (FM), and AFM states as the lowest energy configuration. However, recent inelastic neutron scattering experiments suggested an uninvestigated magnetic structure with ordering along the $[0.5\ 1\ 1]$ plane, motivating a theoretical reinvestigation. Using this insight, we calculated the relative energy of FM and AFM orderings along $[0.5\ 1\ 1]$, $[0.5\ 0\ 0]$, $[0\ 1\ 0]$, and $[0\ 0\ 1]$ using noncollinear DFT calculations with spin-orbital coupling. We found that the $[0.5\ 1\ 1]$ AFM structure is lower in energy than FM or AFM orderings along the low Miller index directions. We also investigated polarization of the magnetic moment along each lattice vector and found that polarization along the out-of-plane direction is the energetically preferred orientation for the AFM structures. Additionally, we found in all calculations that moments initially pointing along the in-plane lattice vectors significantly relax until they point along the coordinate between the two crystallographically distinct uranium sites with complex noncollinear magnetic configurations. The new $[0.5\ 1\ 1]$ AFM magnetic structure provides an additional path forward toward understanding the electronic structure of $\alpha-U_3O_8$ and lends theoretical credibility to recent neutron scattering results.

DOI: [10.1103/PhysRevMaterials.6.104409](https://doi.org/10.1103/PhysRevMaterials.6.104409)

I. INTRODUCTION

Triuranium octoxide (U_3O_8) is prevalent in the nuclear fuel cycle because of its thermodynamic stability at finite temperatures and chemical stability in air. Below approximately 570 K, U_3O_8 assumes an orthorhombic $Amm2$ structure [1,2] with two crystallographically distinct U sites. Several studies agree that the oxidation states in the low-temperature α phase are U(VI) on the U1 site and U(V) on the degenerate U2 sites [3–8]. The U2 sites form a stretched honeycomb lattice, and the U1 sites form a triangular lattice at low temperatures. As shown in Fig. 1, each U1 site lies at the center of the distorted hexagon of U2 sites, and U2 sites sit within an isosceles triangle of U1 sites. However, the U2 sites are located slightly off the centroid of the triangle.

Correctly determining the magnetic structure of $\alpha-U_3O_8$ is a prerequisite for accurate theoretical investigation of the material and complete phenomenological understanding. Nevertheless, consensus about the magnetic structure has not been achieved either experimentally or theoretically, with attempts to elucidate the magnetic structure resulting in a significant number of competing claims. Early experiments found peaks in the magnetic susceptibility at 4.2, 8.0, and 25.3 K [9]. A heat capacity anomaly was also found at 25 K, which was hypothesized as arising from a magnetic transition [8]. Based on heat capacity measurements, U_3O_8 was

reported to be paramagnetic with local magnetic moments of $0.6\ \mu_B$ on the U atoms; however, these experiments encountered considerable issues with reproducibility attributed to nonstoichiometric U_3O_8 samples [8]. The local moment conclusion was supported by Brincat *et al.* who reported that U_3O_8 is paramagnetic based on density functional theory (DFT) calculations with Hubbard $+U$ corrections (DFT $+U$, which is understood to be necessary for open f shell systems) upon finding that several antiferromagnetic (AFM) configurations were isoenergetic [5]. Contrariwise, Wen *et al.* reported that the $[0.5\ 0\ 0]$ AFM configuration with magnetic moments polarized out-of-plane was 6.36 meV/atom lower in energy than the ferromagnetic (FM) state using a similar method [6]. Adding spin-orbit coupling (SOC) corrections to DFT $+U$ calculations, Yun *et al.* [3] and Ranasinghe *et al.* [4] reported an FM ground state, with Ranasinghe assigning the lowest energy magnetic moment direction along the $[0\ 1\ 0]$ direction (the long, in-plane direction); however, Yun *et al.* did not exclude the possibility of a more complex AFM ordering [3].

Recent inelastic neutron scattering (INS) experiments [7] reported AFM ordering below 22 K, which is consistent with the transition temperatures from heat capacity [8] and magnetic susceptibility measurements [9]. Based on the appearance of magnetic scattering peaks in the elastic neutron scattering channel, the suggested AFM ordering is com-

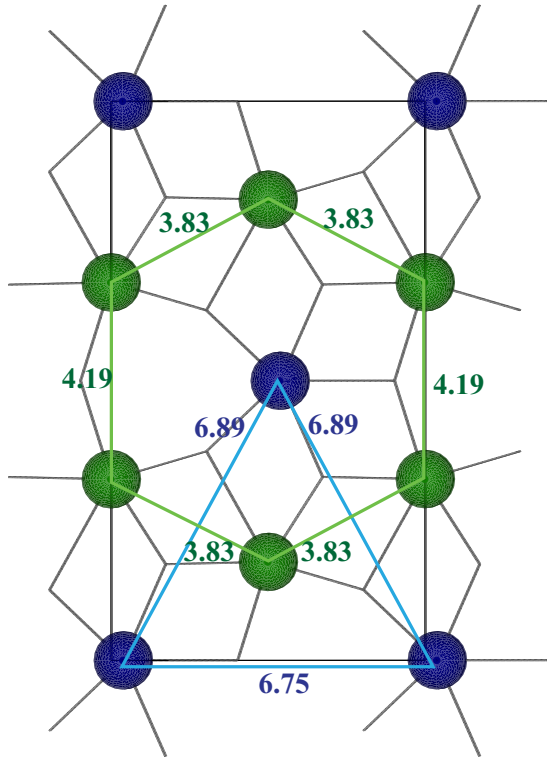


FIG. 1. In-plane α - U_3O_8 lattice depicting the distorted honeycomb formed by U2 sites (green) and the triangle formed by U1 sites (blue).

plex, with a next-neighbor AFM configuration propagating along the out-of-plane lattice direction [7]. These experiments suggested an AFM ordering along the $[0.5\ 1\ 1]$ plane based on geometrical arguments, which is a rather nonintuitive ordering configuration. Notably, no magnetic scattering was observed corresponding to the $[0.5\ 0\ 0]$ AFM configuration, significantly reducing its likelihood of being the correct magnetic ground state configuration, at least above 1.7 K (the baseline temperature accessible in the reported experiments).

In this work, we compared the energetics of the recently proposed $[0.5\ 1\ 1]$ AFM magnetic configuration in U_3O_8 to several FM and AFM orderings ($[0.5\ 0\ 0]$, $[0\ 1\ 0]$, and $[0\ 0\ 1]$) using DFT + U + SOC calculations. We also explicitly investigated polarization of the magnetic moment in the FM and AFM configurations along each crystal lattice vector, which could lead to marked differences in the relative energies of the magnetic structures because of the large anisotropy of the crystal structure between the in-plane and out-of-plane lattice directions.

II. COMPUTATIONAL METHODS

We calculated the relative stability of one FM configuration and four distinct AFM configurations in a $2 \times 1 \times 1$ orthorhombic α - U_3O_8 supercell using DFT with the Vienna *ab initio* Simulation Package (VASP 6.1.1) [10–12]. The PBEsol exchange-correlation functional [13] combined with the projector-augmented wave method [14,15] was used to describe the interatomic interaction. To break the degeneracy

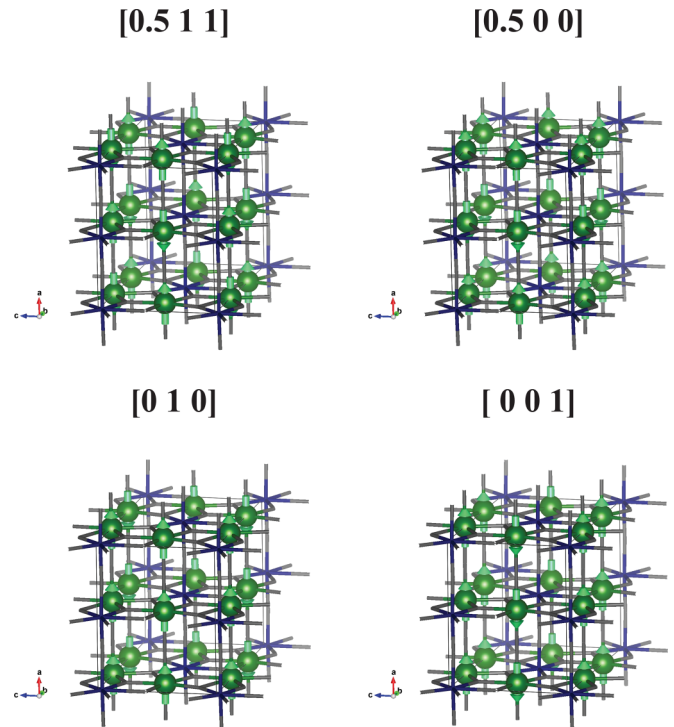


FIG. 2. Initial AFM orderings with magnetic moments initialized along the a axis investigated.

of the f orbitals, an effective Hubbard + U of 4 eV was used, consistent with previous DFT + U studies on U_3O_8 [5,6] and sufficient to provide convergence of lattice energy and magnetic moment in uranium oxide (UO_2) [16]. Without this correction, a metallic electronic ground state is obtained for actinide oxides, which is inconsistent with experiments [17,18]. A k spacing of $0.25\ \text{\AA}^{-1}$ was selected, resulting in 48 k points, to sample the irreducible Brillouin zone with a cutoff energy of 650 eV.

To adequately sample the potential energy surface, we calculated the optimized ionic and magnetic structure of U_3O_8 with magnetic moments initially polarized along the a , b , and c lattice vectors for each magnetic ordering considered, including noncollinear SOC corrections in the structural optimization calculation. The spin axis was set to the default direction of $[0\ 0\ 1]$. Figure 2 shows each AFM ordering with moments initialized along the a lattice vector, which is defined as the out-of-plane direction in this work, consistent with the early work of Loopstra [19]. The full list of initial polarizations for each AFM ordering can be found in the Supplemental Material (SM) (Fig. S1 [20]). In Fig. S1, the naming convention used is $[hkl]-p$ where p denotes along which axis the moments were initially polarized and hkl indicates the Miller index of AFM ordering propagation. The workflow iteratively relaxed the volume and then atomic structure of each system as shown in Fig. S2 in the SM [20], relaxing the electronic and magnetic structure at each step. During the first volume-structure relaxation cycle, orbital occupations were described using Gaussian smearing with an electronic temperature of 0.01 eV, and the energy was converged to a value of 1×10^{-5} eV. The volume

relaxation was stopped once the volume converged, and the atomic relaxation was stopped when the forces were below 1×10^{-3} eV/Å or the energy and forces stopped decreasing. After the first volume-structure relaxation, a second volume-structure relaxation cycle was performed in which the electronic convergence was tightened to 1×10^{-8} eV, and the ionic convergence and smearing values were unchanged. After the second round of relaxations, all ionic forces were less than 1×10^{-3} eV/Å, and the external pressure was less than 0.2 kbar. The final energy of the optimized and converged structure was obtained describing the orbital occupations using the tetrahedron method with Blöchl corrections.

We do not report any calculations in which cell volume, cell shape, and atomic positions relax simultaneously because electronic convergence could not be achieved for these calculations. Consequently, all structures reported in the following discussion are taken from the fourth step in the workflow (Fig. S2 [20]): The atomic position relaxation with energy convergence of 1×10^{-8} eV.

III. RESULTS AND DISCUSSION

In all of the work discussed here, we initialized magnetic moments only on the U2 crystallographic sites because a magnetic moment of $0.0 \mu_B$ has been reported in the literature for the U1 site, commensurate with its +6 oxidation state [3,4,6]. As discussed in detail in Secs. III A–III E, all calculations with moments initially polarized out-of-plane (along a) retain their original AFM or FM magnetic ordering. In the following discussion, we will refer to these magnetic structures as FM- or AFM- $[hkl]$, where hkl denotes the ordering vector. All calculations with magnetic orderings initially polarized in-plane (along b or c) relaxed to states with complex FM and AFM interactions, which are shown in Fig. 3. Notably, the moments form collinear sublattices that are noncollinear with each another. As such, we will refer to these magnetic orderings as noncollinear- n , where n is an arbitrary number given in Fig. 3. Additionally, the AFM magnetic orderings are lower in energy than the noncollinear magnetic orderings, and we discuss the relative energies of the different magnetic structures in Sec. III F.

A. FM ordering

The initial FM orderings consist of all magnetic moments on U2 sites pointing in the same direction along a given lattice vector. Again, no magnetic moment was initialized on the U1 sites. Because a $2 \times 1 \times 1$ supercell is needed to investigate the $[0.5 \ 1 \ 1]$ AFM configuration, we have used the $2 \times 1 \times 1$ supercell in all calculations for consistency. For the initial FM configurations, the magnetic moments are identical in each layer. Only the out-of-plane configuration remained FM after relaxation, and we will refer to this magnetic ordering as FM. In this magnetic structure, the U2 sites had magnetic moments of $+0.76 \mu_B/U$ polarized along a , where the plus sign indicates the moment points in the $+a$ direction (spin up). The orbital and spin components of the magnetic moment were $-1.30 \mu_B/U_2$ and $2.06 \mu_B/U_2$, respectively. Small

antiparallel moments ($< 0.005 \mu_B/U$) were also calculated for U1 sites, which led to a magnetic moment of $-0.02 \mu_B$. The total magnetic moment of the FM configuration was $5.51 \mu_B/\text{supercell}$.

When initially polarized along the b or c lattice vectors, the optimized magnetic moments do not point along the lattice directions, but rather are canted along the shortest U1-U2 direction (Figs. 4 and 5). This results in two U2 magnetic sublattices around each nonmagnetic U1 site, depicted by the red and yellow bars in Fig. 5. The magnetic moments within each sublattice are collinear, but the two sublattices are noncollinear with one another. And although the relaxed magnetic structures are not trivially FM, they do possess FM/AFM ordering along some directions, which was true of all the complex noncollinear orderings calculated in this work. When the magnetic moments were initially polarized along b , the noncollinear-1 magnetic structure is obtained where the relaxed magnetic moments on U2 sites are $+0.27 \mu_B/U$ along b and $\pm 0.63 \mu_B/U$ along c , where the $+c$ and $-c$ components are arranged such that two U2 sites per layer are $+0.63 \mu_B/U$ and the other two U2 sites per layer are $-0.63 \mu_B/U$. Thus, the noncollinear-1 configuration has a net magnetic moment of $2.00 \mu_B/\text{supercell}$ polarized along b because components along c cancel. When moments were initially polarized along c , noncollinear-2 ordering is obtained, where the relaxed magnetic moments on U2 sites are $\pm 0.34 \mu_B/U$ along b and $+0.59 \mu_B/U$ along c . Here, the moments along b cancel so that the net magnetic moment of the supercell points only along c with a magnitude of $4.28 \mu_B/\text{supercell}$.

The complex, noncollinear magnetic configurations shown in Figs. 4 and 5 obtained from the relaxation of FM magnetic arrangements is surprising for several reasons. First, previous investigations of FM ordering did not (to our knowledge) investigate the possibility of noncollinear magnetic orderings. Because we initialized the system with collinear magnetic moments and specifically allowed the noncollinearity to manifest through relaxation, we conclude that magnetic moments prefer to orient along the b/c plane, and strict FM ordering is not the lowest energy magnetic configuration. Second, the difference in energy between the relaxed noncollinear-1 and noncollinear-2 structures is only 0.016 meV/atom—a difference that can be considered essentially degenerate. If such a configuration were to manifest in $\alpha\text{-U}_3\text{O}_8$, significant dynamics between these states should be present. For instance, the net magnetic moment in the relaxed noncollinear-1 case is $2.00 \mu_B$ along the b axis, and in noncollinear-2, it is $4.28 \mu_B$ along c . We would expect transitions between these states to occur readily at any finite temperature. Therefore, dynamics between noncollinear configurations could be highly anisotropic, polarized along the b/c plane. Finally, the magnitude of the differences in net magnetic moments is quite striking— $2.00 \mu_B$, $4.28 \mu_B$, and $5.51 \mu_B$ for noncollinear-1, noncollinear-2, and FM, respectively. The difference in net magnetic moment can be understood partially by a geometric effect—the moments point along the U atom bonds, which are generally arranged about 30° along b from c . In the noncollinear-1 case, the net magnetic moment is a sum over the longer b component of the individual moments on each site; whereas in noncollinear-2, the shorter c component on

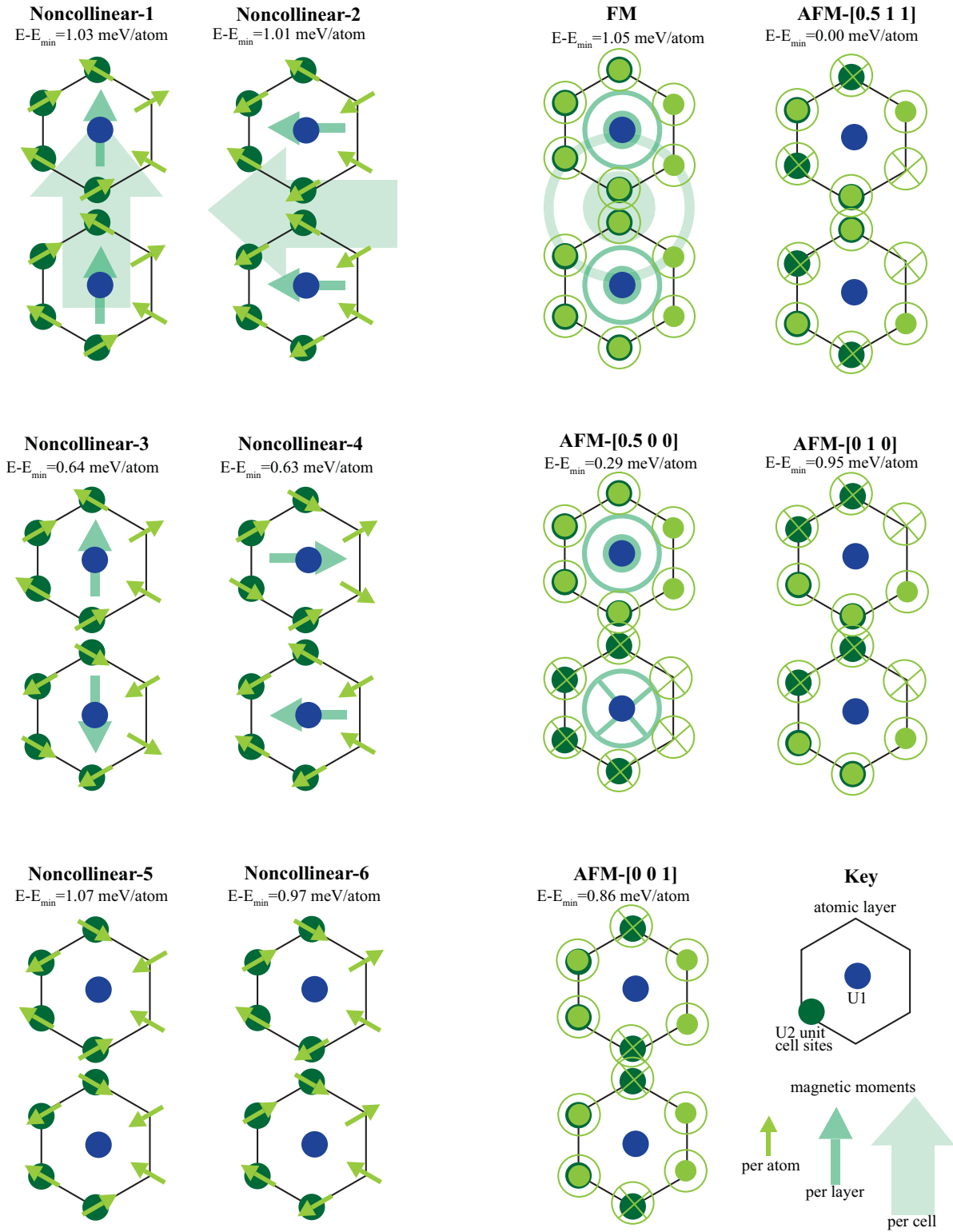


FIG. 3. Schematic of relaxed magnetic structures discussed in the following sections. Two hexagons are given per magnetic ordering, which represent the two atomic layers along a in the $2 \times 1 \times 1$ supercell. Small moment symbols depict magnetic moments on individual atoms, medium symbols within a hexagon denote net magnetic moment of the layer, and large symbols that span two hexagons denote the net magnetic moment of the supercell. Circles with crosses denote moments pointing into the page. No moments are given for layers or supercells with net magnetic moments of $0.0 \mu_B$. Magnetic moments in the noncollinear orderings lie in the bc plane, whereas FM and AFM orderings lie out-of-plane along a . Only U1 and U2 atoms within a single supercell are shown, but magnetic moments are shown for the full U2 hexagon for easier visualization of the magnetic periodicity.

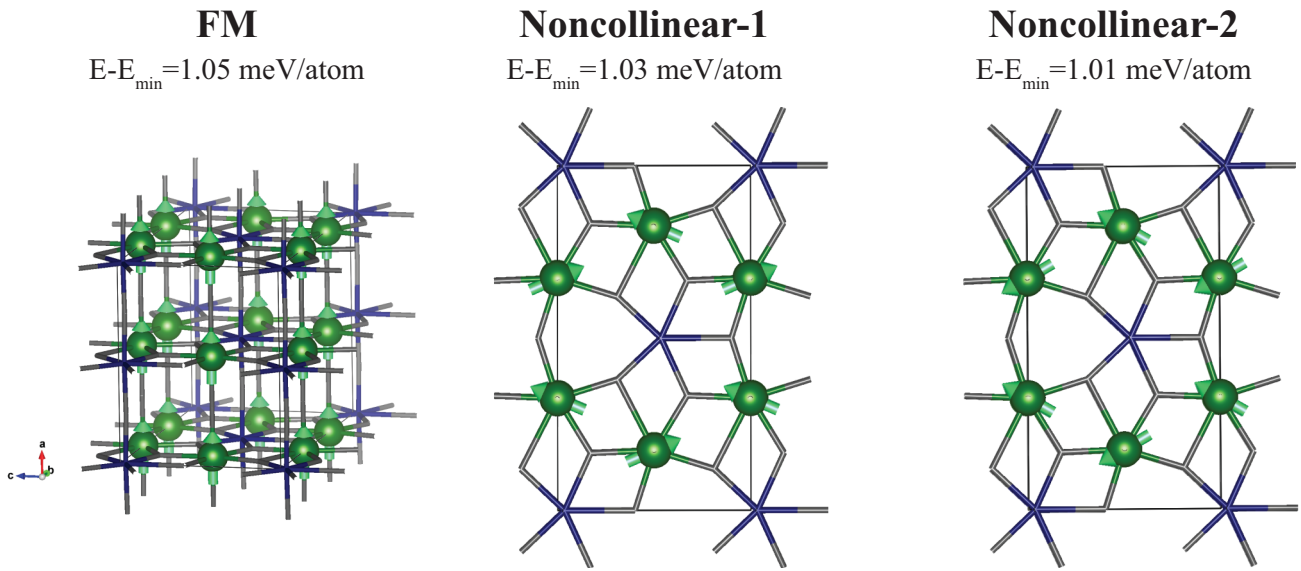


FIG. 4. Final magnetic moments of FM orderings initially polarized along the lattice vectors. The energy relative to the lowest energy magnetic ordering in this work (AFM-[0.5 1 1]) is also given.

each U2 site contributes. To our knowledge, there is no experimental evidence that α -U₃O₈ contains magnetic moments of 2.00–5.5 μ_B /supercell, rendering the noncollinear-1, noncollinear-2, and FM orderings implausible.

B. [0.5 0 0] AFM ordering

In the initial [0.5 0 0] AFM structure, all the magnetic moments on the U2 atoms in a layer point in the same direction. The magnetic moments in the neighboring layers are

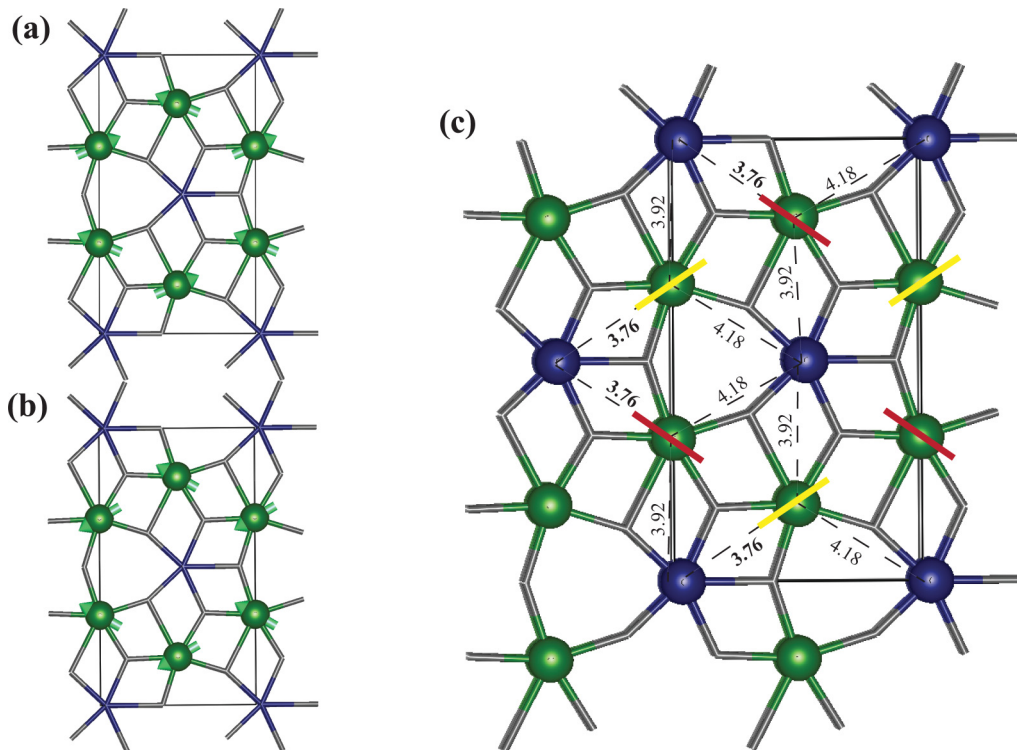


FIG. 5. Top-down view of the noncollinear-1 (a) and noncollinear-2 (b) magnetic structures resultant from an FM initialization. (c) Uranium (V) – uranium (VI) bond distances. Oxygen atoms are shown by grey sticks, and uranium atoms are shown as spheres. Uranium (VI) sites are given in blue, and uranium (V) sites are shown in green. The direction of the shortest uranium (V) – uranium (VI) distance for each uranium (V) site is shown by the solid bars, and the colors distinguish the two U2 magnetic sublattices.

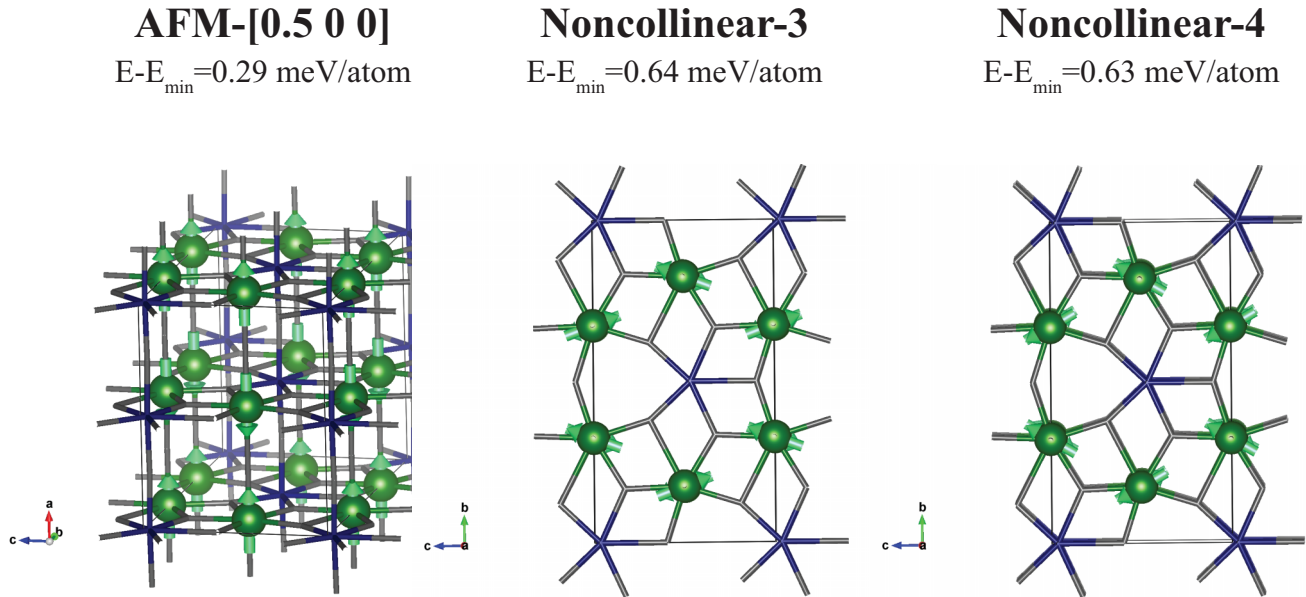


FIG. 6. Final magnetic moments of [0.5 0 0] AFM orderings initially polarized along the lattice vectors. The energy relative to the lowest energy magnetic ordering in this work (AFM-[0.5 1 1]) is also given.

equal in magnitude but opposite in sign so that the overall magnetic moment of the $2 \times 1 \times 1$ supercell system is $0.0 \mu_B$. The optimized magnetic moments on U2 sites when moments are polarized along a are $\pm 0.80 \mu_B/U2$, with orbital and spin components of $\mp 1.32 \mu_B/U2$ and $\pm 2.12 \mu_B/U2$, respectively, and the magnetic ordering is unchanged. We will refer to this ordering as AFM-[0.5 0 0].

When the magnetic moment is initially polarized along b or c , the moments again adopt a canted configuration after relaxation as shown in Fig. 6 and referred to as noncollinear-3 and noncollinear-4. These orderings after relaxation are very similar to the noncollinear-1 and noncollinear-2 magnetic orderings; however, the moments flip between layers for noncollinear-3 and noncollinear-4, leading to net magnetic moments of $0.0 \mu_B/\text{supercell}$ and representing a *net* AFM magnetic ordering along [0.5 0 0]. The optimized components along b and c for the U2 atoms in noncollinear-3 are $\pm 0.25 \mu_B/U$ and $\pm 0.67 \mu_B/U$, respectively. For noncollinear-4, the optimized total magnetic moment components along b and c for the U2 atoms are $\pm 0.35 \mu_B/U$ and $\pm 0.62 \mu_B/U$, respectively. The AFM-[0.5 0 0] structure is 0.35 and 0.34 meV/atom lower in energy than the noncollinear-3 and noncollinear-4 orderings, respectively, and only 0.29 meV/atom higher in energy than the AFM-[0.5 1 1] ordering.

C. [0 1 0] AFM ordering

In the initial [0 1 0] AFM structure, U2 atoms have alternating magnetic moments along the b axis, and the moments across different layers are equivalent. Again we have initially polarized the moments along each lattice direction, and the same behaviors are observed: only the polarization along a (AFM-[0 1 0]) remains unchanged during relaxation, whereas polarization along b and c relax to canted magnetic configurations (noncollinear-5 and noncollinear-6,

Fig. 7). For AFM-[0 1 0], the optimized magnetic moments on U2 sites are $\pm 0.76 \mu_B/U$ along a , with orbital and spin components of ∓ 1.31 and $\pm 2.07 \mu_B/U2$, respectively. The noncollinear-5 structure relaxed to final magnetic moments on U2 sites of $\pm 0.31 \mu_B/U$ along b and $\pm 0.60 \mu_B/U$ along c , but the noncollinear-6 magnetic structure has magnetic moment components of $\pm 0.32 \mu_B/U$ along b and $\pm 0.60 \mu_B/U$ along c . AFM-[0 1 0] is 0.11 meV/atom lower in energy than noncollinear-5 and only 0.01 meV/atom lower in energy than noncollinear-6. However, the AFM-[0 1 0] structure and both noncollinear-5 and noncollinear-6 configurations are significantly higher in energy than the AFM-[0.5 1 1] magnetic ordering.

D. [0 0 1] AFM ordering

In the initial [0 0 1] AFM structure, U2 atoms have alternating magnetic moments along the c axis. Again, initial polarization along the b and c vectors resulted in optimized moments that point along the U1-U2 directions, and the moments remained polarized along a (Fig. 8). In fact, polarization along b and c optimized to the same canted magnetic configurations as initial polarization along c and b , respectively, of the [0 1 0] orderings, namely noncollinear-6 and noncollinear-5. In both the noncollinear-6 and noncollinear-5 structures, the U2 atoms have magnetic moments of $\pm 0.31 \mu_B/U$ or $\pm 0.32 \mu_B/U$ along b and $\pm 0.60 \mu_B/U$ along c . Energy differences of 0.003 meV/atom between noncollinear-6 from initially polarizing the AFM ordering of [0 1 0] along c and [0 0 1] along b and 0.0005 meV/atom between noncollinear-5 calculated from the initial [0 1 0] AFM ordering with moments along b and [0 0 1] ordering with moments along c are negligibly small and confirm that both sets of calculations have converged to the same final magnetic structures. Just like the other AFM orderings in which the moments are polarized along a , the

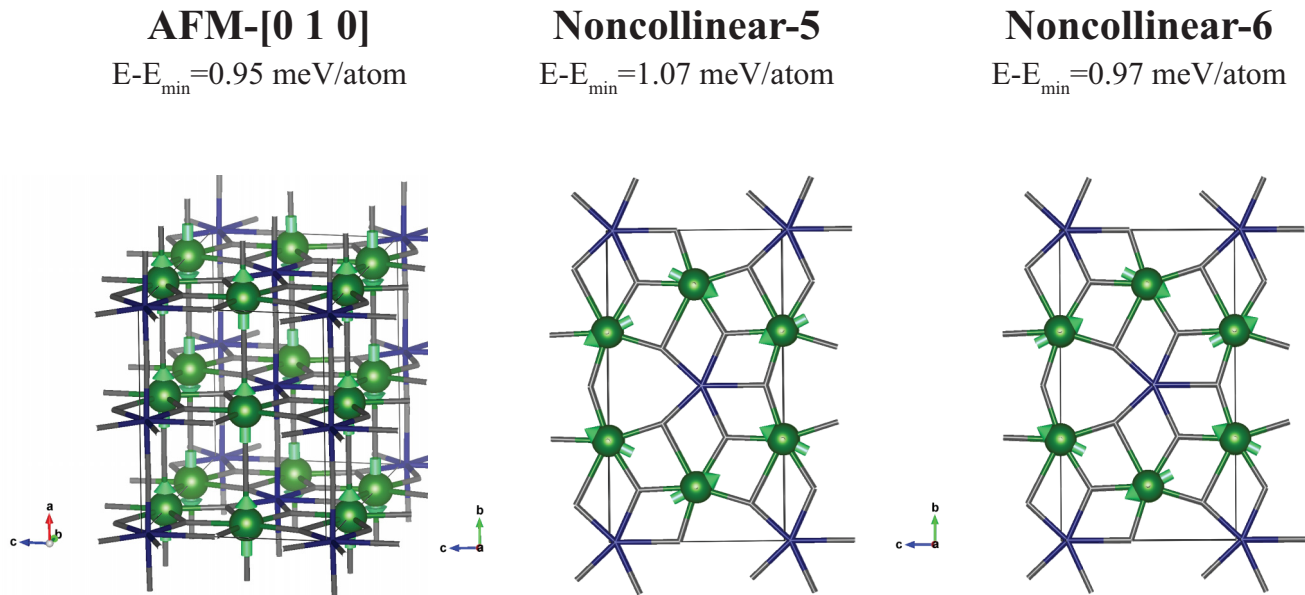


FIG. 7. Final magnetic moments of [0 1 0] AFM orderings initially polarized along the lattice vectors. The energy relative to the lowest energy magnetic ordering in this work (AFM-[0.5 1 1]) is also given.

U2 magnetic moments in AFM-[0 0 1] are $\pm 0.76 \mu_B/U$, and this polarization is lower in energy than the noncollinear-5 and noncollinear-6 orderings by 0.21 and 0.10 meV/atom, respectively. The AFM-[0 0 1] ordering is 0.86 meV/atom higher in energy than the AFM-[0.5 1 1] structure.

E. [0.5 1 1] AFM ordering

In the AFM ordering along [0.5 1 1], as suggested by recent INS experiments [7], the magnetic moments are arranged such that a U2 site is surrounded by U2 sites with antiparallel moments, both in-plane and out-of-plane as shown in Fig. 1

and Fig. S1 in the SM [20]. Again, moments polarized in-plane along *b* optimized along the U1-U2 directions, giving the noncollinear-4 final magnetic configuration (Fig. 9). We also initialized magnetic moments along a U1-U2 direction. Although initially collinear, the optimized magnetic structure is the noncollinear-3 configuration after relaxation. The noncollinear-4 structure has moments of $\pm 0.36 \mu_B/U$ along *b* and $\pm 0.62 \mu_B/U$ along *c*, but the noncollinear-3 structure has slightly smaller moments of approximately $\pm 0.23 \mu_B/U$ or $\pm 0.26 \mu_B/U$ along *b* and slightly larger moments of $\pm 0.67 \mu_B/U$ or $\pm 0.68 \mu_B/U$ along *c*. The noncollinear-3 and noncollinear-4 structures differ from one another in energy by

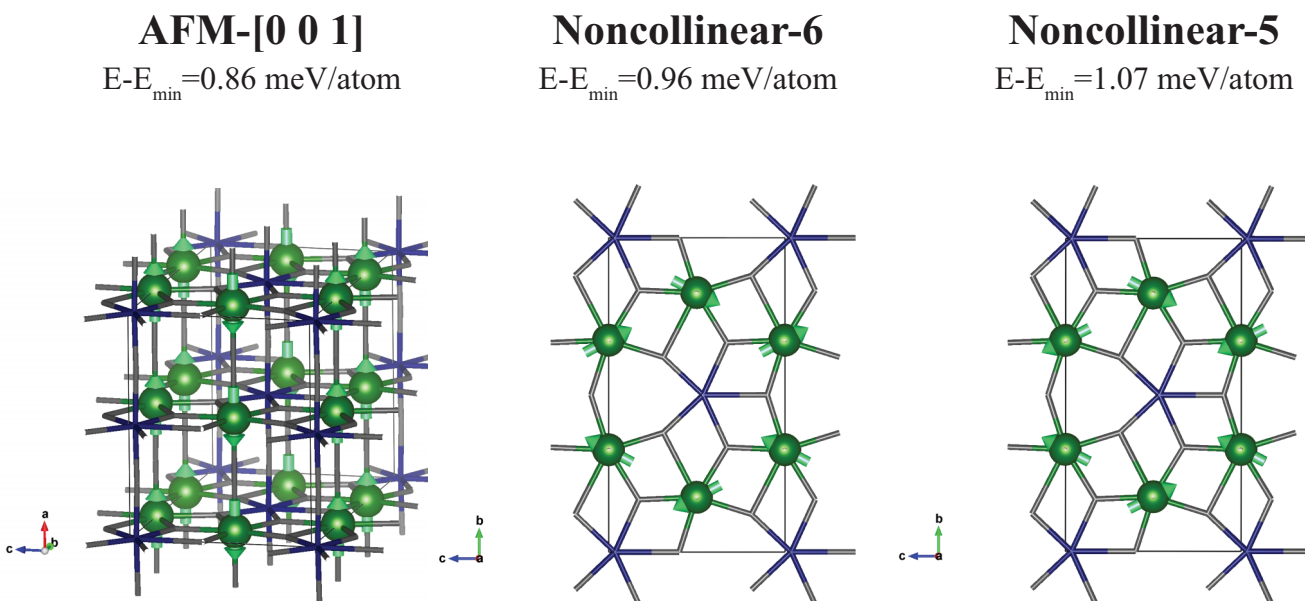


FIG. 8. Final magnetic moments of [0 0 1] AFM orderings initially polarized along the lattice vectors. The energy relative to the lowest energy magnetic ordering in this work (AFM-[0.5 1 1]) is also given.

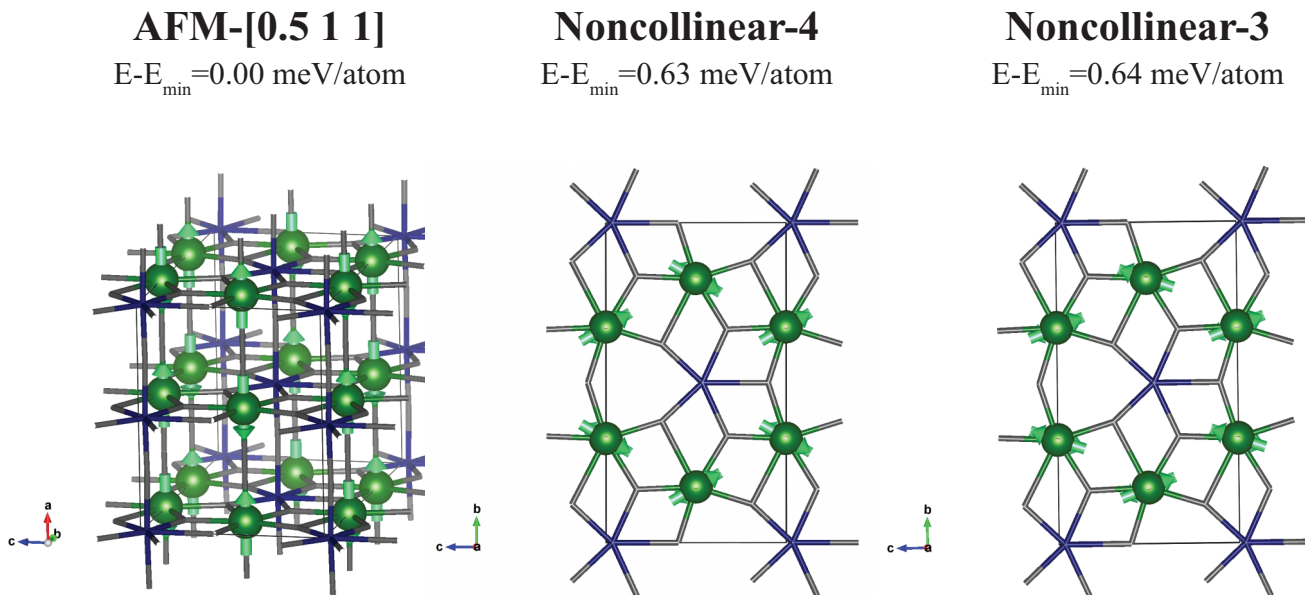


FIG. 9. Final magnetic moments of [0.5 1 1] AFM orderings. The energy relative to the lowest energy magnetic ordering in this work (AFM-[0.5 1 1]) is also given.

only 0.01 meV/atom; however, they are 0.63–0.64 meV/atom higher in energy than the AFM-[0.5 1 1] magnetic configuration. This magnetic structure is the lowest energy magnetic structure calculated and has moments of $\pm 0.81 \mu_B/U$ polarized along a on the U2 sites, slightly larger than the magnetic moments on U2 sites in the other relaxed AFM structures. The magnitude of orbital and spin moments are also larger than the other magnetic configurations, with values of $\mp 1.33 \mu_B/U_2$ and $\pm 2.14 \mu_B/U_2$, respectively.

F. Energetics and electronics

As discussed in Sec. III A, the relaxed noncollinear magnetic orderings are not arbitrary but are canted toward the

nearest U1 site, creating two U2 sublattices around each U1 site (Fig. 5). In noncollinear configurations 1–4, the magnetic moments within each sublattice are ferromagnetically arranged, and the two sublattices within a layer have the same sign for one component of the total magnetic moment. For example, in noncollinear-1, all of the local magnetic moments point along $+b$, and all the local magnetic moments in noncollinear-2 have $-c$ components. Thus, noncollinear-1, noncollinear-2, noncollinear-3, and noncollinear-4 have net magnetic moments within a layer. Noncollinear-1 and noncollinear-2 are also FM along a , leading to a net magnetic moment for the supercell, whereas noncollinear-3 and noncollinear-4 are AFM along a , which gives a net

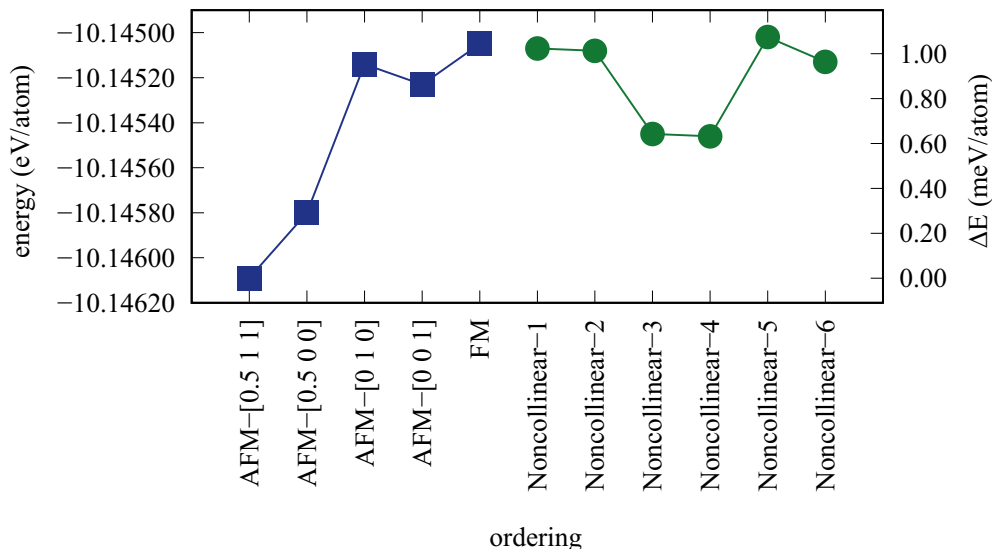


FIG. 10. Energies of the relaxed magnetic orderings investigated. The line connecting the points is meant to guide the eye, and the point colors and shapes are to help distinguish between different classes of magnetic ordering.

TABLE I. Computational method, lowest energy magnetic ordering, magnetic moments on U1 and U2, and electronic band gaps reported in several literature studies.

Author	Software	Functional	U_{eff} (eV)	SOC?	E_{min} ordering	U1/U2 (μ_B)	E_g (eV)
Brincat <i>et al.</i> [5]	VASP	PBE	3.96	no	FM	0.0/1.09	2.19
He <i>et al.</i> [18]	VASP	LDA	4	no	AFM [0.5 0 0]	–	2.43
Ranasinghe <i>et al.</i> [4]	WIEN2K	PBE	4.5	yes	FM	0.0/0.73	2.03
Wen <i>et al.</i> [6]	VASP	PBE	4	no	AFM [0.5 0 0]	0.0/1.1	1.2
Yun <i>et al.</i> [3]	WIEN2K	PBE	4	yes	FM [100]	0.0/0.41	0.50-0.63
Isbill <i>et al.</i> (this work)	VASP	PBEsol	4	yes	AFM [0.5 1 1]	0.0/0.81	1.29

zero magnetic moment for the cell. The U2 sublattices in noncollinear-5 and noncollinear-6 are antiferromagnetically ordered so there is no net magnetic moment even within a layer.

The Gibbs free energy provides insight into the relative thermodynamic stability of the different magnetic orderings, but calculating the free energy requires information about the phonons, which is computationally intractable for the $2 \times 1 \times 1$ supercell at the DFT + U + SOC level used in this work. As such, we are restricted to comparing the electronic energies of the different magnetic orderings, and these energies are given in Fig. 10.

Comparing the energy of each final magnetic ordering, we find the AFM-[0.5 1 1] configuration to have the lowest energy, followed by AFM-[0.5 0 0] (0.29 meV/atom higher). The next lowest energy configurations are noncollinear-3 and noncollinear-4, which are approximately 0.64 meV/atom higher in energy than the AFM-[0.5 1 1] case. The AFM-[0 0 1], AFM-[0 1 0], and FM configurations are 0.86, 0.95, and 1.01 meV/atom higher in energy than the AFM-[0.5 1 1] configuration. The remaining orderings are approximately 1 meV/atom higher in energy than AFM-[0.5 1 1]. Table I provides a summary of our results with those of previous DFT studies from the literature, and key details of the methodology are provided for reference. We have investigated all previously reported minimum-energy magnetic configurations at a consistent level of theory, and the energies of those orderings relative to the AFM [0.5 1 1] ordering are included in Fig. 10.

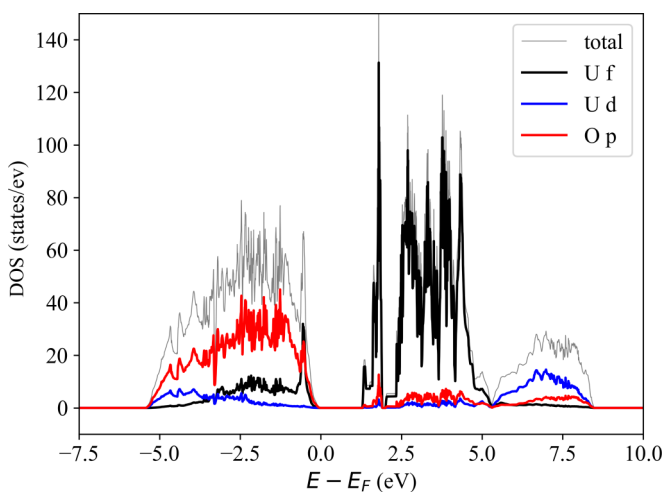


FIG. 11. Electronic density of states of the AFM-[0.5 1 1] ordering in the region near the Fermi energy ($E_F = 0$ eV).

However, now that we have permitted noncollinear ordering to the complex problem of solving the α - U_3O_8 magnetic structure, we acknowledge we have only looked at a small number of the possible magnetic orderings in this system, so we cannot eliminate the possibility of other complex magnetic states lower in energy than the AFM-[0.5 1 1] configuration which could provide further insight into the observed experimental features.

The electronic density of states (eDOS) for the AFM-[0.5 1 1] structure is given in Fig. 11. The valence band is primarily composed of p states on O, d states on U, and f states on U. The partial eDOS reveals the valence f states are on the U2 sites (SM, Fig. S5 [20]). The conduction band is primarily composed of f states on both U1 and U2 sites below 5 eV and p and d states on O and U, respectively, above 5 eV. A 1.29-eV band gap was calculated, in fair agreement with a value between 1.67 and 1.81 eV determined from experimental spectroscopic ellipsometry [18]. The calculated eDOS is also in good agreement with other calculated eDOS for U_3O_8 , despite the difference in magnetic ordering [3,4,6,18]. The only significant difference observed between the eDOS of the different out-of-plane magnetic orderings investigated in this work is the width of the unoccupied p and d bands as shown in Fig. S6 in the SM [20].

IV. CONCLUSIONS

Using DFT + U + SOC calculations, we have calculated the relative energy of FM and AFM configurations along [0.5 0 0], [0 1 0], [0 0 1], and [0.5 1 1] of α - U_3O_8 , considering magnetic moment polarization along each lattice vector. We find that moments initially polarized in-plane along either the b or c lattice vector relax to complex noncollinear configurations that cant along the shortest U1-U2 direction for each U2 site, creating two magnetic sublattices. We find the AFM-[0.5 1 1] ordering, first proposed in recent INS experiments [7], to be the lowest energy magnetic structure. These findings support that the low temperature magnetic ground state of α - U_3O_8 is AFM along [0.5 1 1]. More broadly, these studies highlight a significant potential for nontrivial magnetic effects to contribute to the complex phase behaviors observed in α - U_3O_8 .

ACKNOWLEDGMENTS

This research used resources of the Oak Ridge Leadership Computing Facility, which is a Department of Energy (DOE)

Office of Science User Facility supported under Contract No. DE-AC05-00OR22725. The authors would like to thank Dr. E. Nykwest for helpful discussions. This manuscript has been

authored by UT-Battelle, LLC, under Contract No. DE-AC05-00OR22725 with the U.S. DOE. This work is supported by the National Nuclear Security Administration.

-
- [1] A. Miskowiec, T. Spano, R. Hunt, A. E. Shields, J. L. Niedziela, and S. Finkeldei, Structural features of solid-solid phase transitions and lattice dynamics in U_3O_8 , *Phys. Rev. Mater.* **4**, 093610 (2020).
- [2] R. J. Ackermann, A. T. Chang, and C. A. Sorrell, Thermal expansion and phase transformations of the U_3O_{8-z} phase in air, *J. Inorg. Nucl. Chem.* **39**, 75 (1977).
- [3] Y. Yun, J. Rusz, M. T. Suzuki, and P. M. Oppeneer, First-principles investigation of higher oxides of uranium and neptunium: U_3O_8 and Np_2O_5 , *Phys. Rev. B* **83**, 075109 (2011).
- [4] J. I. Ranasinghe, L. Malakkal, E. Jossou, B. Szpunar, and J. A. Szpunar, Comprehensive study on the electronic and optical properties of $\alpha-U_3O_8$, *Comput. Mater. Sci.* **171**, 109264 (2020).
- [5] N. A. Brincat, S. C. Parker, M. Molinari, G. C. Allen, and M. T. Storr, Density functional theory investigation of the layered uranium oxides U_3O_8 and U_2O_5 , *Dalton Trans.* **44**, 2613 (2015).
- [6] X. D. Wen, R. L. Martin, G. E. Scuseria, S. P. Rudin, E. R. Batista, and A. K. Burrell, Screened hybrid and DFT + u studies of the structural, electronic, and optical properties of U_3O_8 , *J. Phys.: Condens. Matter.* **25**, 025501 (2013).
- [7] A. Miskowiec, T. Spano, Z. E. Brubaker, J. L. Niedziela, D. L. Abernathy, R. D. Hunt, and S. Finkeldei, Antiferromagnetic ordering and possible lattice response to dynamic uranium valence in U_3O_8 , *Phys. Rev. B* **103**, 205101 (2021).
- [8] E. F. Westrum, Jr. and F. Grønvold, Low temperature heat capacity and thermodynamic functions of triuranium octoxide, *J. Chem. Soc.* **81**, 1777 (1959).
- [9] M. J. M. Leask, L. E. J. Roberts, A. J. Walter, and W. P. Wolf, Low-temperature magnetic properties of some uranium oxides, *J. Chem. Soc.* **23**, 4788 (1963).
- [10] G. Kresse and J. Hafner, *ab initio* molecular dynamics for liquid metals, *Phys. Rev. B* **47**, 558 (1993).
- [11] G. Kresse and J. Furthmüller, Efficient iterative schemes for *ab initio* total-energy calculations using a plane-wave basis set, *Phys. Rev. B* **54**, 11169 (1996).
- [12] G. Kresse and J. Furthmüller, Efficiency of *ab-initio* total energy calculations for metals and semiconductors using a plane-wave basis set, *Comput. Mater. Sci.* **6**, 15 (1996).
- [13] G. I. Csonka, J. P. Perdew, A. Ruzsinszky, P. H. T. Philipsen, S. Lebègue, J. Paier, O. A. Vydrov, and J. G. Angyan, Assessing the performance of recent density functionals for bulk solids, *Phys. Rev. B* **79**, 155107 (2009).
- [14] G. Kresse and D. Joubert, From ultrasoft pseudopotentials to the projector augmented-wave method, *Phys. Rev. B* **59**, 1758 (1999).
- [15] P. E. Blöchl, Projector augmented-wave method, *Phys. Rev. B* **50**, 17953 (1994).
- [16] J. Yu, R. Devanathan, and W. J. Weber, First-principles study of defects and phase transition in UO_2 , *J. Phys.: Condens. Matter.* **21**, 435401 (2009).
- [17] B. T. Wang, H. Shi, W. Li, and P. Zhang, First-principles LDA+U and GGA+U study of neptunium dioxide, *Phys. Rev. B* **81**, 045119 (2010).
- [18] H. He, D. A. Andersson, D. D. Allred, and K. D. Rector, Determination of the insulation gap of uranium oxides by spectroscopic ellipsometry and density functional theory, *J. Phys. Chem. C* **117**, 16540 (2013).
- [19] B. O. Loopstra, Neutron diffraction investigation of U_3O_8 , *Acta Crystallogr.* **17**, 651 (1964).
- [20] See Supplemental Material at <http://link.aps.org/supplemental/10.1103/PhysRevMaterials.6.104409> for additional figures.